JCAMECH

Vol. 51, No. 1, June 2020, pp 21-29
DOI: 10.22059/jcamech.2019.282591.406

A theoretical model for analysis of ionic polymer metal composite sensors in fluid environments

Mohammad Reza Salehi Kolahi[a], *Hossein Moeinkhah*[a]*

[a]*Department of Mechanical Engineering, University of Sistan and Baluchestan, Zahedan, Iran*

ARTICLE INFO

Article history:
Received: 31 May 2019
Accepted: 28 June 2019

Keywords:
Dynamic model
IPMC
Physical model
Smart materials

ABSTRACT

By the past two decades IPMCs have been intensively studied because of their special capabilities for actuation and sensing. This paper presents a theoretical physics based model for analyzing the behavior of IPMC sensors in fluid environments. The mechanical vibration of the IPMC strip is described by the classical Euler–Bernoulli beam theory. The model also takes in to account the physical properties of the surrounding fluid. The resulting model is an infinite-dimensional transfer function that relates the input tip displacement to the output sensing current. Further the original model is reduced to a finite-dimensional one, for pure sensing applications of IPMC sensors such as structural health monitoring. The proposed model is verified using existing experimental data. Then the effect of various parameters is investigated. The acoustics physics interface in COMSOL Multiphysics software is used for coupled modal analysis of the IPMC strip. It is shown that the effect of surrounding fluid cannot be neglected.

1. Introduction

In recent years ionic polymer metal composites (IPMCs), which are a unique and new class of smart materials, have been studied by so many theorists and practitioners for their great potential applications in sensing and actuation [1-7]. IPMC sensors are very sensitive to low mechanical stimulus which is an advantage over some piezoelectric sensors. Flexibility, low power consumption, large stroke, excellent biocompatibility and operation in wet environments are some other advantages of the IPMCs [8, 9]. As illustrated in Figure 1, an IPMC is made of a soft ionic polymer membrane sandwiched between thin noble metal electrode layers [10]. Typical polymer membrane materials are Nafion (Perfluorosulfonate) and Flemion (Perfluorocarboxylate) [11] and for the electrodes with high conductivity specification, metals such as platinum, silver and gold can be used [12]. According to the requirements, these groups of smart materials can be made in variety of shapes and sizes [13, 14]. IPMCs are capable of converting energy between chemical, electrical and mechanical domains. Applying a voltage between the conductive electrodes, causes the free cations and attracted water molecules to migrate from the anode to the cathode side. Due to this mechanism, bending motions of the IPMC occur. The polarity of the applied voltage determines the bending direction of the IPMC. Noting that the anions are fixed to the polymer backbone and are not free to move [15, 16]. On the other hand, an applied deformation on an IPMC strip causes redistribution of the free cations inside the polymer and produces a short circuit current across the electrodes [17]. Thus the main cause of both of the actuation and sensing phenomena is induced ionic current.

To study and describe the behavior of IPMCs, up till now several models have been proposed and applied. We can classify these models into three categories as [18]: 1- the black box model, 2- the gray box model and 3- the physical model. The most complex forms among them are physical models, in which the ionic current through the polymer membrane is related to the mechanical deformation [19].

Comparing with the intensive works which have been done on modeling of IPMC actuators, limited researches have been done on IPMC sensors. Based on linear irreversible thermodynamics De Gennes *et al*. [20] proposed a static model to capture both actuation and sensing mechanisms of IPMCs. Farinholt and Leo [21] derived the charge sensing response for a cantilevered IPMC beam under a step change in tip displacement. Chen *et al*. [22] developed a physics-based, geometrically scalable model for IPMC sensors. Their mechanical model was simple and did not include damping effects. They also investigated structural health monitoring capabilities of IPMC sensors. Aureli *et al*. [23] experimentally and theoretically investigated energy harvesting capabilities of base excited IPMC sensors in fluid environments. Their theoretical modeling approach was complicated. In 2011

* Corresponding author. Tel.: +54-31136447; e-mail: hmoein@eng.usb.ac.ir

Ganly *et al*. [24] presented the first systematic studies on temperature-dependent IPMC sensing dynamics. They used a gray box model in form of a forth order transfer function. Lei and Tan [25] developed a dynamic model for a base-excited IPMC sensor operating in air. Using a mathematical model, an estimation of the power harvested by the multilayered cantilever IPMC sensors from the base excitation is reported in [26]. Most of these papers are investigating the features and possible applications of IPMC sensors instead of proposing a complete model.

To the best of our prior studies and knowledge, there is no complete mechanical model for the IPMC sensors. In this research a dynamic, physics based model for analyzing the behavior of the IPMC sensors is presented. This work extends previous studies as it incorporates the effect of the surrounding fluid on the IPMC vibration. The frequency response of an elastic structure is very sensitive to the nature of the fluid in which it is submerged. The deformation of the IPMC is modeled by Euler-Bernoulli beam theory, incorporating viscoelastic damping of the polymer membrane and the surrounding fluid damping force. The description of ion transport dynamics is based on the governing partial differential equation in [22]. Since the resulting model is an infinite-dimensional transfer function, is further reduced to a finite-dimensional one, using some approximations and Taylor series. The resulting model is validated based on the existing experimental data. COMSOL Multiphysics software is used for coupled modal analysis of the IPMC sensor.

The current paper is organized as follows. In section 2, the mathematical model for the IPMC sensor is derived. Model reduction is discussed in section 3. The simulation results are discussed in Section 4. Finally, the conclusions are provided in Section 5.

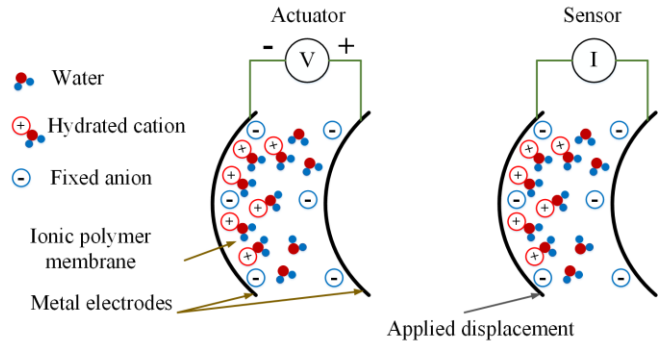

Figure 1. Schematic model of an IPMC strip.

2. Model derivation

Here we consider a slim cantilevered IPMC with rectangular cross section of thickness 2*h*, length *L*, and width *b*. The neutral axis of the beam is shown by $z = 0$, see Figure 2. In order to obtain the dynamic equation of motion we consider the effects that two types of damping have on the frequency response of an elastic structure: viscoelastic damping and damping due to the submergence of the structure in a viscous fluid. The main difference between polymers and other materials resides in the viscoelastic properties of the polymers. Viscoelastic material can be defined as the one whose stress depends on deformation rate [27]. The mechanical response of viscoelastic materials to mechanical excitation has traditionally been modeled in terms of elastic and viscose components such as springs and dashpots. Here we use kelvin-Voigt model. This model combines a spring and a dashpot in parallel, see Figure 3 [28].

$$\sigma_{xx} = Y\left(\varepsilon_{xx} + C_{\mathrm{v}}\frac{\partial \varepsilon_{xx}}{\partial t}\right) \tag{1}$$

here C_{v} denotes the strain rate damping coefficient and Y denotes the Young's modulus.

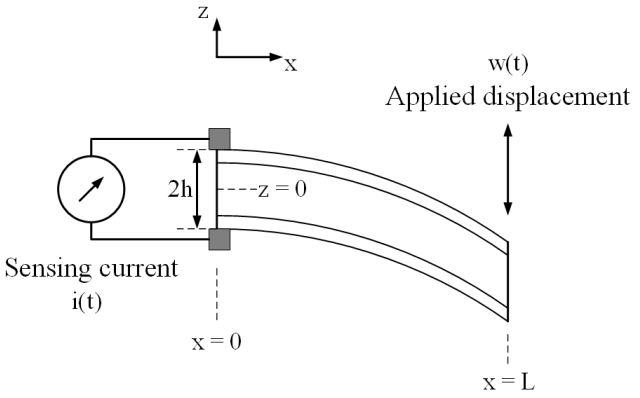

Figure 2. Schematic model of a cantilever IPMC sensor.

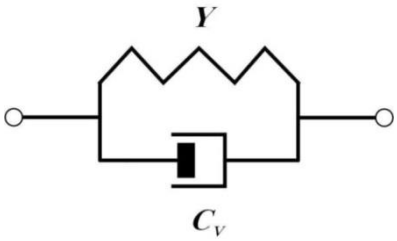

Figure 3. Schematic representation of the Kelvin-Voigt model.

The effect of the damping can be neglected in air, but it cannot be neglected when the cantilever is immersed in a denser medium, like water. The viscous fluid damping force per unit length of the beam can be expressed as [8, 29]

$$f_{\mathrm{fluid}}(x,t) = m_{\mathrm{a}}(\omega)\frac{\partial^2 w(x,t)}{\partial t^2} + C(\omega)\frac{\partial w(x,t)}{\partial t}$$

$$m_{\mathrm{a}}(\omega) = \frac{\rho_f b^2 \pi}{4}\mathrm{Re}\left(\Gamma_{\mathrm{rect}}(\omega)\right) \tag{2}$$

$$C(\omega) = -\frac{\rho_f b^2 \pi}{4}\mathrm{Im}\left(\Gamma_{\mathrm{rect}}(\omega)\right)$$

were ω (rad/s) is the oscillation, $w(x, t)$ is the transverse displacement, b is the width of the IPMC beam, ρ_{f} is the density of the fluid, and $\Gamma_{\mathrm{rect}}(\omega)$ is the hydrodynamic function, $m_a(\omega)$ is the added mass and $C(\omega)$ is the viscous fluid damping coefficient. The hydrodynamic function for a beam with rectangular cross section can be expressed as

$$\Gamma_{\mathrm{rect}}(\omega) = \psi_{\mathrm{corr}}(\omega)\left(1 + \frac{4jK_1\left(-j\left(\sqrt{jR_e}\right)\right)}{\sqrt{jR_e}K_0\left(-j\left(\sqrt{jR_e}\right)\right)}\right) \tag{3}$$

where K_0 and K_1 are modified Bessel functions of the second type, $\psi_{\text{corr}}(\omega)$ is a complex valued correction function that corrects the results for a beam of circular cross section to a beam of rectangular cross section and

$$R_e = \frac{\rho_f \omega b^2}{4\mu_f} \tag{4}$$

where R_e is the Reynolds number and μ_f is the viscosity of fluid. The correction function for the rectangular cross section is given by [30]

$$\psi_{\text{corr}} = \psi_r(\omega) + j\psi_i(\omega) \tag{5}$$

where

$$\begin{aligned} \psi_r(\omega) &= \frac{a_r}{b_r} \\ \psi_i(\omega) &= \frac{a_i}{b_i} \end{aligned} \tag{6}$$

and

$$\begin{aligned} a_r &= 0.91324 - 0.48274\lambda + 0.46842\lambda^2 \\ &\quad - 0.12866\lambda^3 + 0.044055\lambda^4 \\ &\quad - 0.0035117\lambda^5 + 0.00069085\lambda^6 \\ b_r &= 1 - 0.56964\lambda + 0.48690\lambda^2 \\ &\quad - 0.13444\lambda^3 + 0.045155\lambda^4 \\ &\quad - 0.0035862\lambda^5 + 0.00069085\lambda^6 \\ a_i &= -0.024134 - 0.029256\lambda \\ &\quad + 0.016294\lambda^2 - 0.00010961\lambda^3 \\ &\quad + 0.000064577\lambda^4 - 0.00004451\lambda^5 \\ b_i &= 1 - 0.59702\lambda + 0.55182\lambda^2 \\ &\quad - 0.18375\lambda^3 + 0.079156\lambda^4 \\ &\quad - 0.014369\lambda^5 + 0.0028361\lambda^6. \end{aligned} \tag{7}$$

The quantity λ is defined as

$$\lambda = \log_{10} R_e \tag{8}$$

Expression (3) of the hydrodynamic function can be used for a wide range of Reynolds numbers [30]. Considering these assumptions, the governing equation of motion is obtained as [31]

$$\begin{aligned} &\eta(\omega)\frac{\partial^2 w(x,t)}{\partial x^2} + C(\omega)\frac{\partial w(x,t)}{\partial x} \\ &\quad + C_v I \frac{\partial^5 w(x,t)}{\partial x^4 \partial t} + YI\frac{\partial^4 w(x,t)}{\partial x^4} = 0 \end{aligned} \tag{9}$$

where $\eta(\omega) = \rho_m A + m_a(\omega)$, ρ_m is the density, A is the cross sectional area of IPMC and I is the area moment of inertia with respect to the x axis. By converting equation (9) into the Laplace domain we have

$$(Y + C_v I)\frac{\partial^4 w(x,s)}{\partial x^4} + \left(C(\omega) + \eta(\omega)s^2\right)w(x,s) = 0 \tag{10}$$

where s is the Laplace variable. Equation (10) can be rewritten as

$$\frac{\partial^4 w(x,s)}{\partial x^4} + 4\gamma^4(s)s^2 w(x,s) = 0 \tag{11}$$

where $\gamma^4(s)$ is

$$\gamma^4(s) = \frac{C(\omega) + \eta(\omega)s}{4Is(Y + C_v s)} \tag{12}$$

The general solution for equation (11) is as follows [32]

$$\begin{aligned} w(x,s) &= A_1(s)\cos(px)\cosh(px) \\ &\quad + A_2(s)\cos(px)\sinh(px) \\ &\quad + A_3(s)\sin(px)\cosh(px) + A_4(s)\sin(px)\sinh(px) \end{aligned} \tag{13}$$

where

$$p = \gamma\sqrt{s} \tag{14}$$

For the clamped-free boundary conditions, the following relations can be obtained.

$$\begin{aligned} &w(0,s) = 0\ ,\ \frac{\partial w(0,s)}{\partial x} = 0 \\ &w(L,s) = W(s)\ ,\ \frac{\partial^2 w(L,s)}{\partial x^2} = 0 \end{aligned} \tag{15}$$

By substituting the boundary conditions into (13), we get

$$w(x,s) = \frac{A(x,s)}{B(s)}W(s) \tag{16}$$

where

$$\begin{aligned} A(x,s) &= \cos(px)\sinh(px) - \sin(px)\cosh(px) \\ &\quad + C(s)\left(\sin(px)\sinh(px)\right) \\ B(s) &= \cos(pL)\sinh(pL) - \sin(pL)\cosh(pL) \\ &\quad + \frac{\sin(pL)\sinh(pL)}{\cos(pL)\cosh(pL)} \\ &\quad \times\left(\sin(pL)\cosh(pL) + \cos(pL)\sinh(pL)\right) \\ C(s) &= \frac{\sin(pL)\cosh(pL) + \cos(pL)\sinh(pL)}{\cos(pL)\cosh(pL)} \end{aligned} \tag{17}$$

As illustrated in Figure 2, an applied displacement $w(t)$ leads to the generation of the sensing current $i(t)$ due to redistribution of the free cations. The governing PDE which describes the charge density distribution ρ within the polymer membrane is given by [22]:

$$\begin{aligned} &\frac{\partial \rho(x,z,t)}{\partial t} - d\frac{\partial^2 \rho(x,z,t)}{\partial x^2} \\ &\quad + \frac{F^2 dC_0}{\varepsilon RT}(1 - C_0\Delta V)\rho(x,z,t) = 0 \end{aligned} \tag{18}$$

where d is the ionic diffusion, F is Faraday's constant, R is the gas constant, T is the absolute temperature, ε is the effective dielectric constant of the polymer membrane, C_0 is the anion

concentration, and ΔV is the molar volume change. By taking the Laplace transform for the of $\rho(x, z, t)$, we can convert (18) into the frequency domain as

$$\frac{\partial^2 \rho(x,z,s)}{\partial x^2} + \beta^2(s)\rho(x,z,s) = 0 \tag{19}$$

where $\beta^2(s)$ is

$$\beta^2(s) = \frac{s+k}{d} \quad , \quad k = \frac{F^2 dC_0}{\varepsilon RT}(1 - C_0 \Delta V) \tag{20}$$

Assuming that the charge density is symmetric relative to $z = 0$, the solution of (19) is obtained as

$$\rho(x,z,s) = 2a_1(x,s)\sinh(\beta(s)z) \tag{21}$$

The following equations describe the electric field E and the electric potential φ.

$$E(x,z,s) = -\frac{\partial \varphi(x,z,s)}{\partial x} \tag{22}$$

$$\varepsilon \frac{\partial E(x,z,s)}{\partial x} = \rho(x,z,s) \tag{23}$$

With the above equations and equation (21), we can evaluate $E(x, z, s)$ and $\varphi(x, z, s)$ as

$$E(x,z,s) = 2a_1(x,s)\frac{\cosh(\beta(s)z)}{\varepsilon\beta(s)} + b_1(x,s) \tag{24}$$

$$\varphi(x,z,s) = -2a_1(x,s)\frac{\sinh(\beta(s)z)}{\varepsilon\beta^2(s)} - b_1(x,s)z + b_2(x,s) \tag{25}$$

The charge density $\rho(\pm h, z, s)$ inside the polymer membrane at the boundary $z = \pm h$ is proportional to the induced stress $\sigma(\pm h, z, s)$ [33]:

$$\sigma(x,\pm h,s) = \alpha\rho(x,\pm h,s) \tag{26}$$

where α is the charge–stress coupling constant. Now we can relate the induced stress $\sigma(x, h, s)$ to the external stimulus $W(s)$. According to linear beam theory we have

$$\sigma(x,z,s) = \frac{M(x,s)z}{I} \quad , \quad M(x,s) = YI\frac{\partial^2 w(x,s)}{\partial x^2} \tag{27}$$

where M is the bending moment. Substituting the equation (16) in to (27) one can obtain the stress at $z = h$

$$\sigma(x,h,s) = \frac{YhW(s)}{B(s)}\frac{\partial^2 A(x,s)}{\partial x^2} \tag{28}$$

Using equation (26) we can get $a_1(x, s)$

$$a_1(x,s) = \frac{YhW(s)}{2\alpha B(s)\sinh(\beta(s)h)}\frac{\partial^2 A(x,s)}{\partial x^2} \tag{29}$$

Now we can obtain $b_1(x, s)$ and $b_2(x, s)$ using the short circuit boundary condition $\varphi(x, h, s) - \varphi(x, -h, s) = 0$.

$$b_1(x,s) = -2a_1(x,s)\frac{\sinh(\beta(s)h)}{\varepsilon h\beta^2(s)} \quad , \quad b_2(x,s) = 0 \tag{30}$$

By integrating the electric displacement field $D = \varepsilon E$ over the cross section of the beam at the $z = h$ the total induced electric charge can be obtained as

$$Q(s) = \int_0^b \int_0^L \varepsilon E(x,h,s)\,dx\,dy \tag{31}$$

The short-circuit current $i(t)$ in the Laplace domain is $i(s) = sQ(s)$. Finally we can achieve to the transfer function which relates the mechanical input $w(s)$ to the output sensing current $i(s)$ as

$$H(s) = \frac{I(s)}{W(s)} = \frac{Ybs\left(\beta(s)h\coth(\beta(s)h) - 1\right)}{\alpha\beta^2(s)} \times \frac{1}{B(s)}\int_0^L \frac{\partial^2 A(x,s)}{\partial x^2} \tag{32}$$

where

$$\int_0^L \frac{\partial^2 A(x,s)}{\partial x^2} = -2p\sin(pL)\sinh(pL) + pC(s)\left(\cos(pL)\sinh(pL) + \sin(pL)\cos(pL)\right) \tag{33}$$

3. Reduced order model

The resulting model in equation (33), is infinite-dimensional as it contains nonrational terms like sin(○), cos(○) and $\sqrt{\circ}$, etc. For practical implementation of the model, such as structural health monitoring, we aim to reduce the model to a finite order. First, we take $1 - C_0\Delta V \approx 1$ since $|C_0\Delta V\frac{k}{d}| \ll 1$. Based on the data listed in Table 1, for $s = j\omega$, the term $\frac{k}{d}$ is of the order of 10^{12}, which means

$$|\beta(s)| = \left|\frac{s+k}{d}\right| \geq 10^6 \tag{34}$$

On the other hand, due to the thickness of the sensor it can be concluded that

$$|\beta(s)h| \gg 10 \tag{35}$$

Equation (34) allows us to consider the following approximation

$$H_1(s) = \frac{Ybs\left(\beta(s)h\coth(\beta(s)h) - 1\right)}{\alpha\beta^2(s)} = \frac{Ybs\left(\beta(s) - 1\right)}{\alpha\beta^2(s)} = \frac{Ybs\sqrt{d}\left(\sqrt{s+k} - \sqrt{d}\right)}{\alpha(s+k)} \tag{36}$$

Further we can approximate the term $\sqrt{s+K}$ using its Taylor series about $s = 0$. The following approximation can be achieved by considering up to the second order.

$$H_1(s)=\frac{Ybs\sqrt{d}\left(h\sqrt{k}\left(1+\frac{s}{k}\right)-\sqrt{d}\right)}{\alpha(s+k)} \tag{37}$$

To simplify the second part of (32), Taylor series expansion for terms sin(○), cos(○), sinh(○) and cosh(○) will be used. Considering just the first three terms in each series leads to equation (39).

$$H_2(s)=\frac{5\left((pL)^{16}-128(pL)^{12}-384(pL)^{8}\right.}{L\left((pL)^{16}-56(pL)^{12}-10560(pL)^{8}\right.} \\ \frac{\left.+36864(pL)^{4}+8294400\right)}{\left.+576000(pL)^{4}+27648000\right)} \tag{38}$$

The resulting finite-dimensional approximation is

$$\tilde{H}(s)=H_1(s)\cdot H_2(s) \tag{39}$$

4. Results and discussion

In order to verify the obtained model, parameters in the model need to be identified. Some parameters in the model are physical constants (gas constant R and Faraday constant F) and some of them such as sensor dimensions, temperature T, density ρ_m and young modulus Y are directly measurable. The other parameters must be identified through a curve fitting process in MATLAB [8]. The MATLAB function *fminsearch* can be used to find the remaining parameters. This command minimizes the squared error between the experimental frequency response and the proposed model prediction. Table 1 shows the proposed model parameters. The frequency response of the proposed model is obtained for an IPMC sensor with the same dimensions, 22 × 7 × 0.360 mm^3, as used by Chen *et al*. [22]. By substituting $s = j2\pi f$ in equation (32) and using MATLAB the Bode plot of the frequency response can be obtained. Figure 4 shows the Bode plot of the frequency response. As illustrated in Figure 4, there is a good correlation between the proposed model and experimental results. This indicates that the proposed model is effective in capturing the sensing of the IPMC.

It is worth noting that Chen *et al*. [22] conducted their experiments in air. As the proposed model is a physical model it is geometrically scalable. Thus we can study the effects of geometrical parameters. Figure 5 shows the effect of length variation on the sensor's behavior. The length variation affects only the magnitude and has not any effect on the phase. It also can be seen that as the strip gets longer the magnitude decreases. It means that the output sensing current decreases too. Next we investigate the effect of hydration level on the IPMC sensor behavior. Humidity variation leads to changes in diffusion coefficient d. Figure 6 shows and compares the predicted frequency response for three different diffusion coefficients d.

Table 1. Model parameters

C_0	1091 (mol/m^3)
C_v	20000(Pa.s)
d	1.2×10^{-11} (m^2/s)
F	96487 (C/mol) [22]
R	8.3143 (J/mol.K) [22]
T	300 (K) [22]
Y	571 (MPa) [22]
ε	2.2 (mF/m)
ρ_m	9159.3 (kg/m^3) [22]
α	109 (J/C)

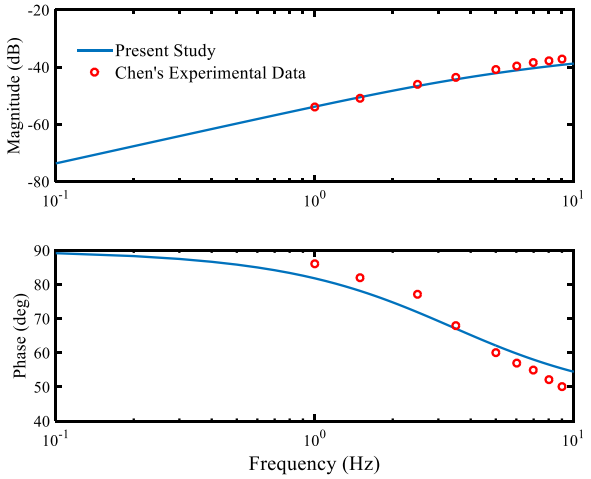

Figure 4. Comparison of the frequency response with experimental data.

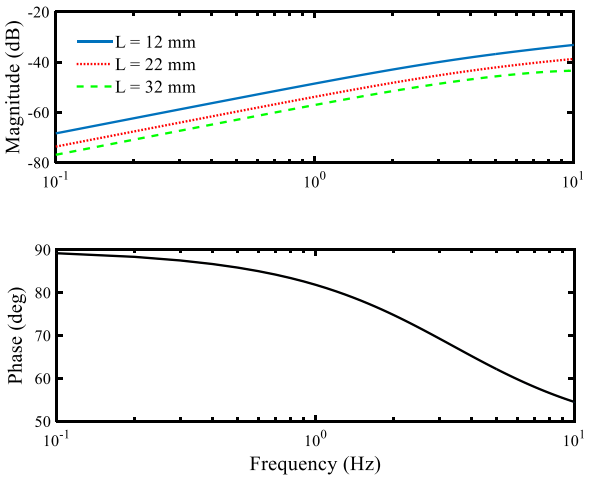

Figure 5. The effect of length variation.

When the IPMC sensor is oprating in air, it faces with water evaporation and its hydration level decreases and the diffusion coefficient decreases too. Figure 7 shows the cyclic current–displacement plot. This plot corresponds to a harmonic mechanical tip-displacement with peak of 1 mm and frequency of 10 Hz. The overall behavior of the sensor in figure 7 is the same as figure 6, as the diffusion coefficient decreases the output sensing current gets smaller.

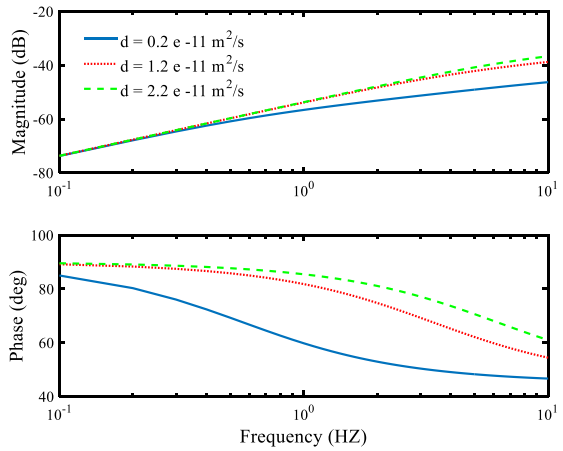

Figure 6. The effect of diffusion coefficient variation.

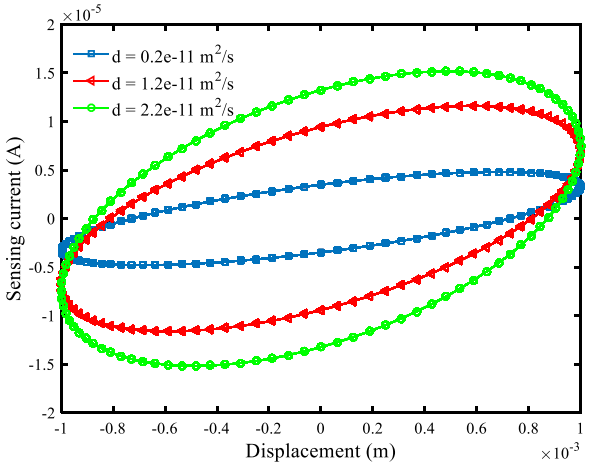

Figure 7. Current-displacement cyclic diagram.

The natural frequencies of a cantilever beam submerged in a viscous fluid, can be obtained by the following equation [34]

$$\omega_{\text{fluid}}^{n} = \omega_{\text{vac}}^{n}\left(1+\frac{\pi\rho_{\text{f}}b}{4\rho_{\text{m}}h}\Gamma_{\text{rect}}\left(\omega_{\text{vac}}^{n}\right)\right)^{-1/2} \tag{40}$$

where ω_{vac} is the natural frequency in vacuum. As the IPMCs can be used in wet conditions and are biocompatible we investigate and compare their behavior in water and human blood as well as air. The first coupled natural frequency of the IPMC sensor submerged in air, deionized water and human blood is given in Table 2. Noting that the boundary conditions, geometrical and physical parameters are the same as figure 4. The values are captured from COMSOL Multiphysics software and equation (40). Table 3 summarizes the characteristics of the mentioned fluids.

Table 2. Evaluation of the first coupled natural frequency (Hz)

Fluid	Analytical Eq. (40)	FE	Experimental [22]
Air	29.975	32.013	~30
Deionized water	18.3861	21.00	–
Human blood	17.6907	20.282	–

Table 3. Fluid properties of Table 2

Fluid	ρ_{f} (kg.m^{-3})	μ_{f} (Pa.s)
Air	1	0.0001
Deionized water	997	0.0008
Human blood	1125	0.004

The acoustics physics interface in COMSOL Multiphysics software can be used to compute the coupled natural frequencies of an elastic structure submerged in a fluid. We used a three dimensional geometry for simulation. It is worth noting that the used mesh is free triangular with 78154 elements. We selected this type and number of mesh after several simulations.

According to the Table 2, there is a fine correlation between analytical and FE simulation results. In particular with denser fluid, the natural frequency is lower. The changes in the natural frequency values enable us to realize resonant sensors. Now we investigate the effect of the surrounding fluid on the sensors frequency response. Figure 8 shows and compares the frequency response of the sensor submerged in three different mediums. It is clear that the effect of the surrounding fluid cannot be neglected specially for the vibrating frequencies more than 1 Hz.

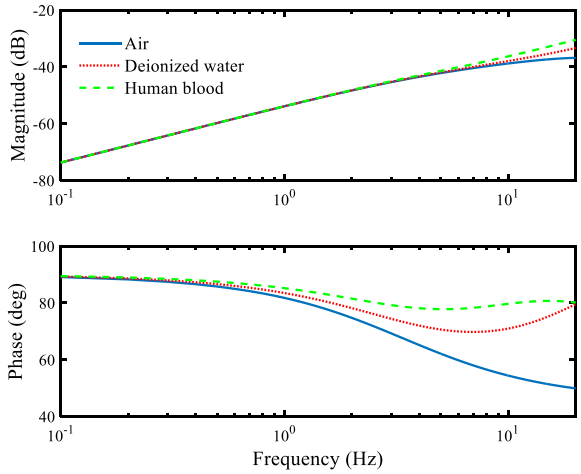

Figure 8. Comparison of the frequency response for three different mediums.

For some sensing applications like structural health monitoring (SHM), our aim is to reconstruct the original mechanical signal $u(t)$ based on the output sensing current $i(t)$. The reconstructed mechanical signal can be achieved by inverting the reduced order model.

$$H_{\text{inv}} = \frac{W(s)}{I(s)} = \frac{1}{\tilde{H}(s)} \tag{41}$$

It shows also the wide applicability of the proposed model. Figures 9 to 11 show the reconstructed signal for three different sensing currents. Figure 9 shows a smooth step excitation leads to a sensing current which rises to a peak value and then decreases to zero. For figures 10 and 11 reconstructed signal and sensing current are similar. It means a decay oscillatory excitation leads to a decay oscillatory current and a multitone oscillatory excitation leads to a multitone oscillatory current.

5. Conclusions

In current paper a theoretical model which is physics-based, is proposed to simulate the mechano-electrical response of IPMC sensors. Moreover, the model accommodates the effect of the surrounding fluid on the IPMC sensing. Since the original model is an infinite-dimensional transfer function, it is not suitable for some applications. Further the order of the original model is reduced and converted to a rational transfer function. It is shown that the resulting model has a fine correlation with the existing experimental data.

More the effect of various parameters investigated. The results showed that as the sensor gets longer, the output sensing current gets smaller. Results also depicted that decreasing the hydration level leads to reduction of output sensing current. It has also been observed that the effect of the surrounding fluid cannot be neglected. We used acoustics physics interface in COMSOL Multiphysics software for modal analysis. Results showed that the IPMCs natural frequency differs from one medium to another. This change enables one to use IPMC sensors as resonant sensors. On the other hand the reduced order model enables one to use IPMC sensors for structural health monitoring, especially for underwater structures.

The results of this paper could be of interest in a number of applications. In fact, it is possible to use the proposed model as a project tool for designing sensors. Future work will involve the effects of the time varying temperature on the sensors behavior. It is also possible to consider the surface electrode resistance into to the modeling approach.

(a)

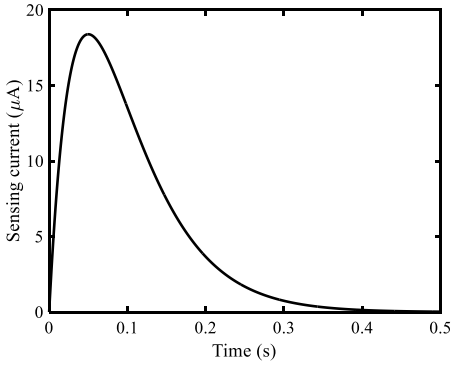

(b)

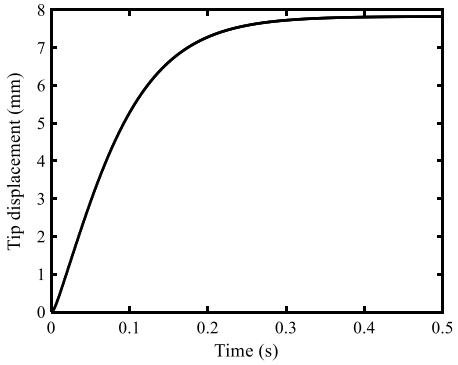

Figure 9. Desired sensing current (a), reconstructed signal: step excitation (b).

(a)

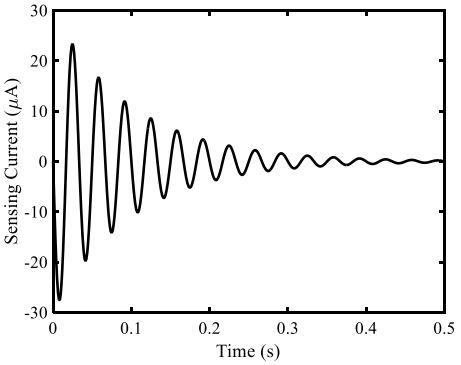

(b)

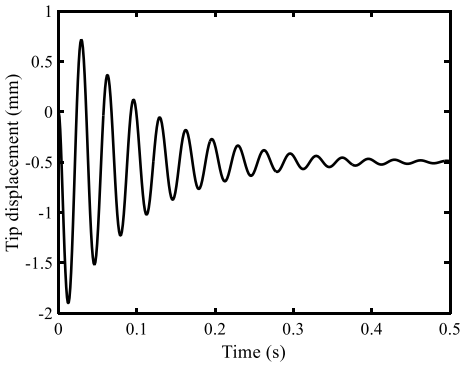

Figure 10. Desired sensing current (a), reconstructed signal: decay oscillatory excitation (b).

(a)

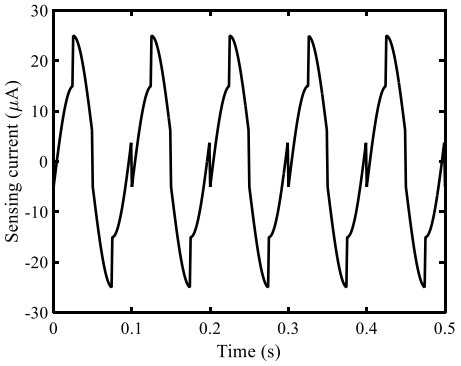

(b)

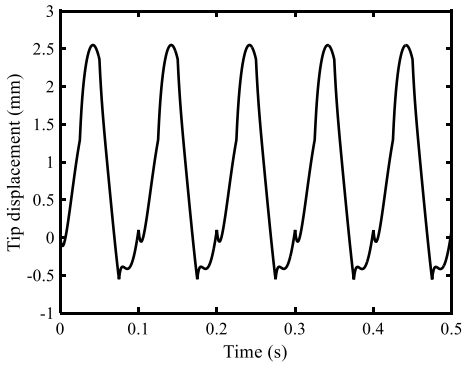

Figure 11. Desired sensing current (a), reconstructed signal: multitone oscillatory excitation (b).

6. References

[1] M. Porfiri, H. Sharghi, P. Zhang, Modeling back-relaxation in ionic polymer metal composites: The role of steric effects and composite layers, *Journal of Applied Physics*, Vol. 123, No. 1, pp. 014901, 2018.

[2] H. Liu, K. Xiong, K. Bian, K. Zhu, Experimental study and electromechanical model analysis of the nonlinear deformation behavior of IPMC actuators, *Acta Mechanica Sinica*, Vol. 33, No. 2, pp. 382-393, 2017.

[3] X. Chen, C.-Y. Su, Adaptive control for ionic polymer-metal composite actuators, *IEEE Transactions on Systems, Man, and Cybernetics: Systems*, Vol. 46, No. 10, pp. 1468-1477, 2016.

[4] I. Dominik, J. Kwaśniewski, F. Kaszuba, Ionic polymer-metal composite displacement sensors, *Sensors and Actuators A: Physical*, Vol. 240, pp. 10-16, 2016.

[5] D. Bandopadhya, Application of Lambert W-function for solving time-delayed response of smart material actuator under alternating electric potential, *Proceedings of the Institution of Mechanical Engineers, Part C: Journal of Mechanical Engineering Science*, Vol. 230, No. 13, pp. 2135-2144, 2016.

[6] D. Biswal, D. Bandopadhya, S. Dwivedy, Electro-mechanical and thermal characteristics of silver-electroded ionic polymer–metal composite actuator, *Proceedings of the Institution of Mechanical Engineers, Part C: Journal of Mechanical Engineering Science*, Vol. 226, No. 6, pp. 1427-1436, 2012.

[7] M. Shahinpoor, Y. Bar-Cohen, J. Simpson, J. Smith, Ionic polymer-metal composites (IPMCs) as biomimetic sensors, actuators and artificial muscles-a review, *Smart materials and structures*, Vol. 7, No. 6, pp. R15, 1998.

[8] H. Moeinkhah, J.-Y. Jung, J.-H. Jeon, A. Akbarzadeh, J. Rezaeepazhand, K. Park, I.-K. Oh, How does clamping pressure influence actuation performance of soft ionic polymer–metal composites?, *Smart Materials and Structures*, Vol. 22, No. 2, pp. 025014, 2013.

[9] D. Pugal, P. Solín, K. Kim, A. Aabloo, hp-FEM electromechanical transduction model of ionic polymer–metal composites, *Journal of Computational and Applied Mathematics*, Vol. 260, pp. 135-148, 2014.

[10] Q. Shen, V. Palmre, T. Stalbaum, K. J. Kim, A comprehensive physics-based model encompassing variable surface resistance and underlying physics of ionic polymer-metal composite actuators, *Journal of Applied Physics*, Vol. 118, No. 12, pp. 124904, 2015.

[11] Y. Bar-Cohen, S. Leary, A. Yavrouian, K. Oguro, S. Tadokoro, J. Harrison, J. Smith, J. Su, Challenges to the transition of IPMC artificial muscle actuators to practical application, 1999.

[12] M. Shahinpoor, K. J. Kim, Ionic polymer-metal composites: I. Fundamentals, *Smart materials and structures*, Vol. 10, No. 4, pp. 819, 2001.

[13] H. Moeinkhah, J. Rezaeepazhand, A. Akbarzadeh, I.-K. Oh, Accurate dynamic modeling of helical ionic polymer-metal composite actuator based on intrinsic equations, *IEEE/ASME Transactions on Mechatronics*, Vol. 20, No. 4, pp. 1680-1688, 2015.

[14] R. Tiwari, K. Kim, Disc-shaped ionic polymer metal composites for use in mechano-electrical applications, *Smart Materials and Structures*, Vol. 19, No. 6, pp. 065016, 2010.

[15] D. Pugal, K. J. Kim, A. Aabloo, An explicit physics-based model of ionic polymer-metal composite actuators, *Journal of Applied Physics*, Vol. 110, No. 8, pp. 084904, 2011.

[16] D. Pugal, K. J. Kim, A. Punning, H. Kasemägi, M. Kruusmaa, A. Aabloo, A self-oscillating ionic polymer-metal composite bending actuator, *Journal of Applied Physics*, Vol. 103, No. 8, pp. 084908, 2008.

[17] H. Lei, M. A. Sharif, X. Tan, Dynamics of omnidirectional IPMC sensor: Experimental characterization and physical modeling, *IEEE/ASME Transactions on Mechatronics*, Vol. 21, No. 2, pp. 601-612, 2016.

[18] H. Moeinkhah, J. Rezaeepazhand, A. Akbarzadeh, Analytical dynamic modeling of a cantilever IPMC actuator based on a distributed electrical circuit, *Smart Materials and Structures*, Vol. 22, No. 5, pp. 055033, 2013.

[19] Z. Chen, X. Tan, A Control-Oriented and Physics-Based Model for Ionic Polymer--Metal Composite Actuators, *IEEE/ASME Transactions on Mechatronics*, Vol. 13, No. 5, pp. 519-529, 2008.

[20] P. De Gennes, K. Okumura, M. Shahinpoor, K. J. Kim, Mechanoelectric effects in ionic gels, *EPL (Europhysics Letters)*, Vol. 50, No. 4, pp. 513, 2000.

[21] K. Farinholt, D. J. Leo, Modeling of electromechanical charge sensing in ionic polymer transducers, *Mechanics of Materials*, Vol. 36, No. 5-6, pp. 421-433, 2004.

[22] Z. Chen, X. Tan, A. Will, C. Ziel, A dynamic model for ionic polymer–metal composite sensors, *Smart Materials and Structures*, Vol. 16, No. 4, pp. 1477, 2007.

[23] M. Aureli, C. Prince, M. Porfiri, S. D. Peterson, Energy harvesting from base excitation of ionic polymer metal composites in fluid environments, *Smart materials and Structures*, Vol. 19, No. 1, pp. 015003, 2009.

[24] T. Ganley, D. L. Hung, G. Zhu, X. Tan, Modeling and inverse compensation of temperature-dependent ionic polymer–metal composite sensor dynamics, *IEEE/ASME Transactions on Mechatronics*, Vol. 16, No. 1, pp. 80-89, 2011.

[25] H. Lei, C. Lim, X. Tan, Modeling and inverse compensation of dynamics of base-excited ionic polymer–metal composite sensors, *Journal of Intelligent Material Systems and Structures*, Vol. 24, No. 13, pp. 1557-1571, 2013.

[26] M. Patel, S. Mukherjee, Modelling and Analysis of Ionic Polymer Metal Composite based Energy Harvester, *Materials Today: Proceedings*, Vol. 5, No. 9, pp. 19815-19827, 2018.

[27] H. F. Brinson, L. C. Brinson, Polymer engineering science and viscoelasticity, *New York: Springer*, Vol. 66, pp. 79, 2008.

[28] D. Gutierrez-Lemini, 2014, *Engineering viscoelasticity*, Springer,

[29] P. Brunetto, L. Fortuna, S. Graziani, S. Strazzeri, A model of ionic polymer–metal composite actuators in underwater

operations, *Smart materials and Structures*, Vol. 17, No. 2, pp. 025029, 2008.

[30] J. E. Sader, Frequency response of cantilever beams immersed in viscous fluids with applications to the atomic force microscope, *Journal of applied physics*, Vol. 84, No. 1, pp. 64-76, 1998.

[31] E. B. Magrab, 2012, *Vibrations of elastic systems: With applications to MEMS and NEMS*, Springer Science & Business Media,

[32] S. S. Rao, 2007, *Vibration of continuous systems*, Wiley Online Library,

[33] S. Nemat-Nasser, J. Y. Li, Electromechanical response of ionic polymer-metal composites, *Journal of Applied Physics*, Vol. 87, No. 7, pp. 3321-3331, 2000.

[34] C. A. Van Eysden, J. E. Sader, Resonant frequencies of a rectangular cantilever beam immersed in a fluid, *Journal of applied physics*, Vol. 100, No. 11, pp. 114916, 2006.